RSC Mechanochemistry

ROYAL SOCIETY OF CHEMISTRY

COMMUNICATION

View Article Online
View Journal | View Issue

Cite this: *RSC Mechanochem.*, 2025, **2**, 188

Received 7th October 2024
Accepted 17th December 2024

DOI: 10.1039/d4mr00118d

rsc.li/RSCMechanochem

Synthesis of a thermally stable 2D MOF *via* neat grinding and annealing of a panel-like triangular ligand with Zn(II)†

Stefano Elli, Manfredi Caruso, Alessandro Sacchetti and Javier Martí-Rujas *

A new exotridentate ligand, 1,3,5-tris(2-methylpyridin-4-yl)benzene (mTPB), was synthesized and self-assembled with $ZnBr_2$ in the solid-state *via* mechanochemistry (*i.e.*, neat grinding (NG)), followed by annealing. The amorphous phase generated by NG transformed into a crystalline structure corresponding to a 2D MOF (1) through an amorphous-to-crystalline transition. Compound 1 contains open 2D layers and exhibited thermal stablility up to 300 °C. Analogous 1,3,5-tris(pyridyl)benzene (TPB), upon NG, formed a poly-[*n*]-catenane of interlocked ($M_{12}L_8$) nanocages. This different behaviour was attributed to the presence of the methyl groups in the mTPB ligand.

Introduction

Mechanochemistry is an important synthetic route that contributes to the development of a cleaner chemistry as it does not require solvents and can be applied to a wide variety of materials.[1–7] Recently, the first solid-state reactivity involving the tridentate 2,4,5-tris(4-pyridyl)benzene (**TPB**)[8–11] and 2,4,5-tris(4-pyridyl)triazine (**TPP**)[12] ligands for the synthesis of 1D poly-[*n*]-catenanes self-assembled from interlocked $M_{12}L_8$ metal–organic cages (PC-MOCs)[13] has been reported. In the solid state, changes in the aromaticity of the central ligands **TPB** and **TPP** lead to different products, which are attributed to the varying efficiency of π–π interactions involved in the mechanical bonds that form the polycatenanes.[13] The functionalization of the **TPP** ligand with a Cl group at the 3-position of the 4′-pyridyl ring has been studied with ZnI_2 in the solution state.[14,15] It was observed that a 1D coordination polymer was formed instead of the poly-[*n*]-catenanes composed of interlocked $M_{12}L_8$ nanocages. This different behavior was attributed to the steric hindrance caused by the Cl atom appended to the **TPP** ligand.[14]

To date, there are no reports on the effect of **TPB** ligand functionalization on the formation of mechanically interlocked $M_{12}L_8$ nanocages and its solid-state reactivity using mechanochemistry. Harvesting experimental data on the factors that prevent or promote the formation of topologically intriguing systems such as PC-MOCs[16] and MOFs is fundamental for expanding our understanding of the structural and coordination chemistry of rigid triangular pyridine-based ligands and advancing the development of functional materials.[17–22]

Herein, the synthesis of a new high-symmetric (C_3-symmetry) trimethylated TPB ligand, 1,3,5-tris(2-methylpyridin-4-yl)benzene (**mTPB**), and its self-assembling behaviour with $ZnBr_2$ in the solid-state have been reported. The reaction was carried out by neat grinding (NG) followed by annealing. The mechanochemical reaction led to an amorphous phase (**a1**), which exhibited short-range order, as indicated by the diffuse scattering observed in the powder XRD pattern. Amorphous **a1** transformed into a crystalline material upon thermal annealing, yielding a novel 2D MOF (**1**), which was characterized by single crystal XRD (SC-XRD). The 2D MOF was found to consist

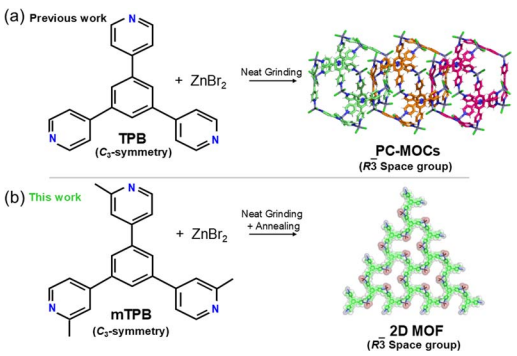

Fig. 1 Schematic representation of the different products obtained in the self-assembling of PC-MOCs and 2D MOFs obtained upon slow crystallization.

Dipartimento di Chimica Materiali e Ingegneria Chimica. "Giulio Natta", Politecnico di Milano, Via L. Mancinelli 7, 20131 Milan, Italy. E-mail: javier.marti@polimi.it

† Electronic supplementary information (ESI) available. CCDC 2389166 and 2388980. For ESI and crystallographic data in CIF or other electronic format see DOI: https://doi.org/10.1039/d4mr00118d

of porous layers featuring a minimum circuit of six ligands and six metals and was thermally stable up to 300 °C (Fig. 1).

The results showed that the methyl groups in the pyridine rings drove the formation of a 2D MOF instead of a poly-[*n*]-catenane composed of mechanically interlocked $M_{12}L_8$ nanocages. This experimental work provides valuable insights into the conditions that influence the formation of mechanically interlocked systems, such as $M_{12}L_8$ polycatenanes (PC-MOCs), as well as 2D MOFs.

Results and discussion

Synthesis of mTPB ligand

The C_3 symmetry exotridentate ligand **mTPB** was synthesized through a Suzuki–Miyaura coupling (see ESI†). Three methyl-substituted pyridines were attached to the benzene ring by cross-coupling their boronated derivatives with tribromobenzene. The crude product was purified by column chromatography and characterized using NMR, mass spectrometry, IR, SC-XRD and powder XRD techniques (see ESI†). A single crystal of **mTPB** was obtained by evaporation of a chloroform solution of **mTPB** and analysed by SC-XRD. **mTPB** crystallizes in the triclinic space group $P\bar{1}$ with unit cell parameters (100 K): $a = 7.8599(2)$ Å; $b = 10.2595(3)$ Å; $c = 13.1951(4)$ Å; $\alpha = 85.688(3)°$; $\beta = 89.484(3)°$; $\gamma = 75.632(3)°$; $V = 1027.79$ Å^3. In the asymmetric unit, there is one **mTPB** and two water molecules. The water molecules form 1D channels along the *a*-axis that fill 11.8% of the total unit cell volume (Fig. 2).

In the solid state, the distance between the two **mTPB** molecules is 4.052 Å (distance calculated between the centroids of the central benzene rings). The angles between the planes of the benzene rings and the pyridines are $\theta_1 = 41.95°$, $\theta_2 = 43.20°$ and $\theta_3 = 25.82°$ (Fig. 2). The torsions of the methylated pyridine rings are due to the presence of the methyl group and the repulsion between pyridinic and benzenic H···H atoms. The powder XRD pattern of the obtained microcrystalline matches well with the simulated SC-XRD (see ESI†), indicating that the **mTPB** single crystal is representative of the bulk powder.

In **mTPB** there are various types of hydrogen bonds. First, there are the ones established between the electron-rich nitrogen of one pyridine group of the **mTPB** molecule that interacts with the hydrogen of a water molecule within approximately 1.986 Å (–N···H–O–H). Also, there are hydrogen bonds among water molecules (H–O···H–O–H, 1.971 Å). Then, there are short contacts between the pyridine nitrogen and the hydrogen of the benzene ring of a neighbouring **mTPB** molecule (–N···H-Benz, 2.645 Å) or with the hydrogen of the pyridine ring of a neighbouring **mTPB** molecule (–N···H-Py, 2.719 Å).

Solid-state reactivity of mTPB and $ZnBr_2$ by mechanochemistry followed by heating

Thermal reactivity has been shown to be a fruitful approach in the formation of unique topologies including amorphous-to-crystalline transformations but also to study solid-state reactivity in MOFs.[23–27] The solid-state chemistry of **mTPB** has also been explored for the first time by carrying out a mechanochemical reaction by NG followed by annealing. The NG experiment resulted in an amorphous phase without starting **mTPB**, suggesting that it reacted with $ZnBr_2$ (Fig. 3a). The powder XRD diffractogram of the NG product resembles that observed in the solid-state synthesis of poly-[*n*]-catenanes self-assembled interlocked $M_{12}L_8$ MOCs.[7,9] The diffractogram shows two large bumps at $2\theta/° \approx 14$ and 26, indicating that in the product had some short-range ordering (Fig. 3a). Interestingly, in the powder XRD pattern there is no presence of the initial **mTPB**, indicating that it reacted with $ZnBr_2$. To maintain the solid-state process, in the absence of solvents, heat was used to proceed with the reaction.

Thus, the amorphous solid **a1** obtained in the NG process was further annealed to 300 °C for one hour and cooled to ambient temperature for *ca.* 4 h. The powder XRD diffractogram of **a1** shows that the sample became crystalline with several Bragg reflections (Fig. 3b). **a1** was microcrystalline but showed low resolution to attempt the structure solution from powder

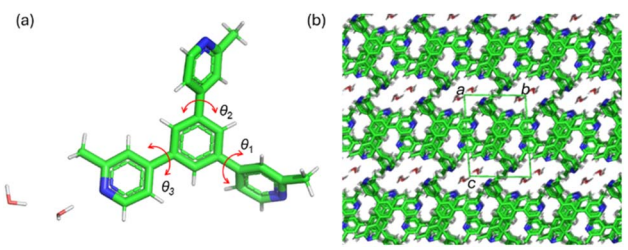

Fig. 2 (a) SC-XRD structure of **mTPB** ligand used in this work in its dihydrated form showing the asymmetric unit. (b) Crystal packing of dihydrated **mTPB** viewed along the crystallographic *a*-axis.

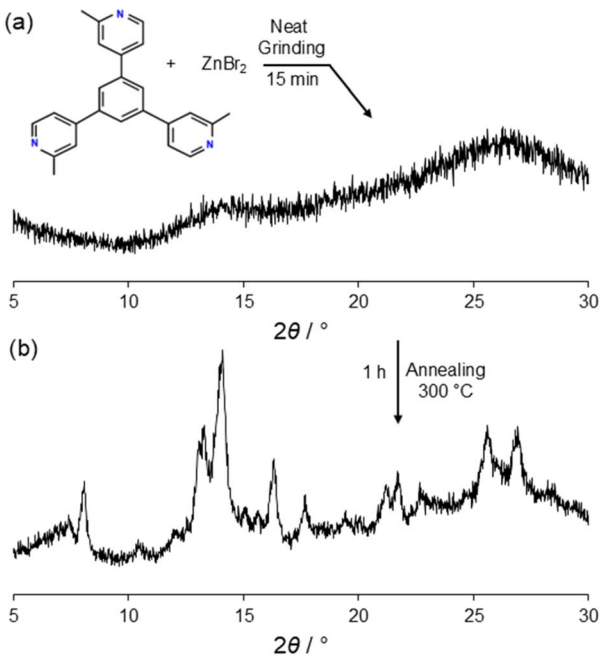

Fig. 3 Powder XRD patterns of the product obtained after NG **mTPB** and $ZnBr_2$ (a) and diffractogram of the annealed sample obtained upon NG (b).

XRD.[28,29] To understand the crystalline structure obtained by NG and annealing of **a1**, we tried to grow a single crystal by mixing **mTPB** and $ZnBr_2$.

In a crystallization tube, single crystals suitable for SC-XRD were prepared by layering **mTPB** at the bottom in a 1,2-dichlorobenzene solution, methanol as the central layer, and the metal salt as a top layer (see ESI†). $ZnBr_2$ was added dropwise to avoid rapid precipitation. After three days, large crystals (hereafter **1**) were formed. One single crystal, stable at room temperature, was taken and measured by SC-XRD.

SC-XRD shows that **1** is a MOF and includes disordered methanol crystallizing in the trigonal space group $R\bar{3}$ with the crystallographic formula $(C_{16}H_{14}Br_2N_2Zn)\cdot(MeOH)$. The asymmetric unit is composed of a $ZnBr_2$ coordinated to one-third of **L** (Zn···N) twice and contains one disordered methanol molecule. The unit cell parameters are (302 K) $a = 21.4323(2)$ Å; $b = 21.4323(2)$ Å; $c = 19.3803(2)$ Å; $\alpha = 90°$; $\beta = 90°$; $\gamma = 120°$; $V = 7709.54(16)$ Å^3. It is important to note that the trigonal space group is the same as that of the $M_{12}L_8$ poly-[*n*]-catenanes.

The 2D layers are defined as porous layers in which the window openings are large. The minimum circuit formed of ligand and $ZnBr_2$ contains six **mTPB** ligands and six metal centers. In the coordinated **mTPB**, the two angles between the planes containing the benzene rings and pyridines are $\theta_1 = 38.71°$ and $\theta_2 = 35.18°$. The 2D layers stack one on top of each other expanding along the *c*-axis. The stacking of layers does not yield a channel structure due to the translation of adjacent layers. The open space in a single layer has an internal opening of 8.4 Å (Br–Br) and 17.3 Å (Br–CH_3) (Fig. 4c).

In the stacking layers, there are three different distances among the centers of the rings (*i.e.*, 4.023 Å, 4.047 Å and 7.264) as shown in Fig. 4d. While the first two contacts can be considered π–π interactions, the longest one cannot be considered as such due to the guest inclusion. Therefore, these aromatic interactions do not expand continuously along the *c*-axis, which would be important to study the electron conductivity.[30] About the short contacts established in **1**, the bromide atoms form weak electrostatic interactions with the hydrogens of the pyridines (Py-H···Br–Zn, 2.959 Å). These interactions are responsible for keeping the 2D planes stacked together. Importantly there is no interaction involving any methyl groups with adjacent layers or guests.

Voids analysis showed that the space occupied by the solvent corresponds to 7% (531 Å^3) of the total unit cell volume (spherical probe with a 1.2 Å radius).[31] The voids in **1** are below the central benzene rings of **mTPB** and there are three per unit cell, which are not connected (Fig. S9†).

The crystallization tube was monitored for one month, and it was observed that a microcrystalline powder was deposited at the bottom. The powder XRD of the solid matched that simulated from **1**, indicating that the selected single crystal **1** is representative of the bulk powder (Fig. 5a). Thus, no other crystalline phases were formed with **1** after long crystallization periods using the stratification method.

An important aspect of the 2D reported is the weak interlayer interactions observed in **1** that opens exfoliation studies.[32] It should be possible to create 2D nanosheets with potential applications in various areas due to the presence of large voids in the 2D structure.

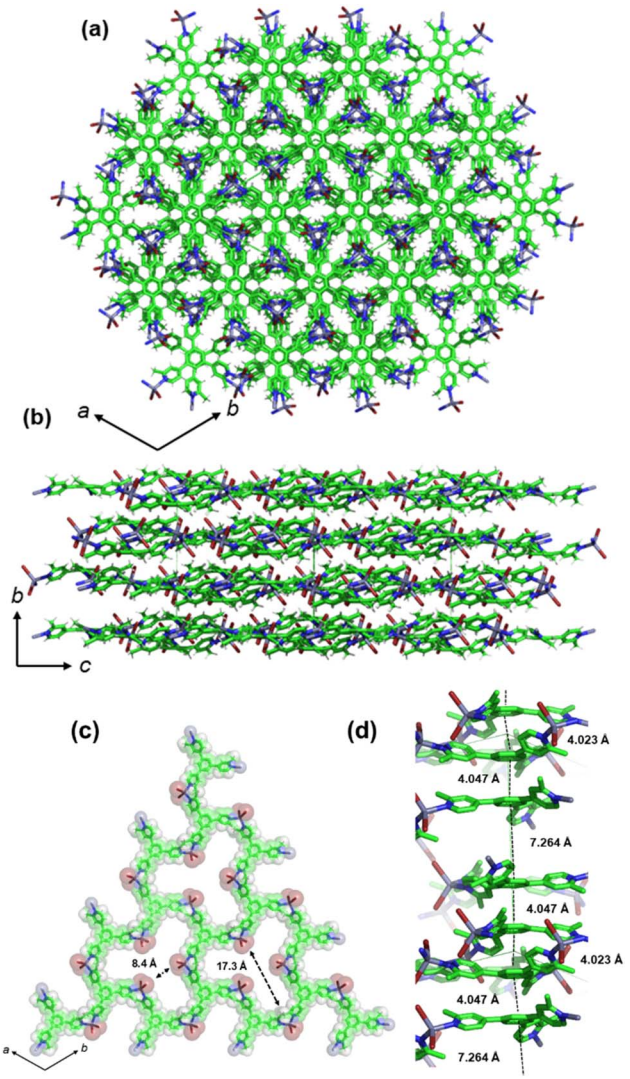

Fig. 4 Crystal structure of **1** viewed along the stacking direction (a) and perpendicular to it (b). A portion of a 2D layer in **1** demonstrating the open nature of a single layer (c). Detailed view of the aromatic–aromatic (benzene) distances along the *c*-axis. Solvent molecules have been omitted for clarity.

Thermal stability of 1

A crucial point of a given 2D MOF is its stability. Thus, the thermal stability of the 2D MOF was also monitored by annealing **1** up to 300 °C for 1 h in an oven and then measured by *ex situ* powder XRD. The diffractogram shows that **1** is still very crystalline and the diffraction pattern did not change indicating that the same structure is maintained (Fig. 5). In fact, thermogravimetric (TG) analysis shows that **1** is stable until 400 °C and afterwards it starts to decompose (Fig. S11†). This good thermal stability is important for the potential applications of this type of layered MOF materials.

The annealing effect promoted the self-assembly of **mTPB** and $ZnBr_2$ to form the layered structure. This solid-state

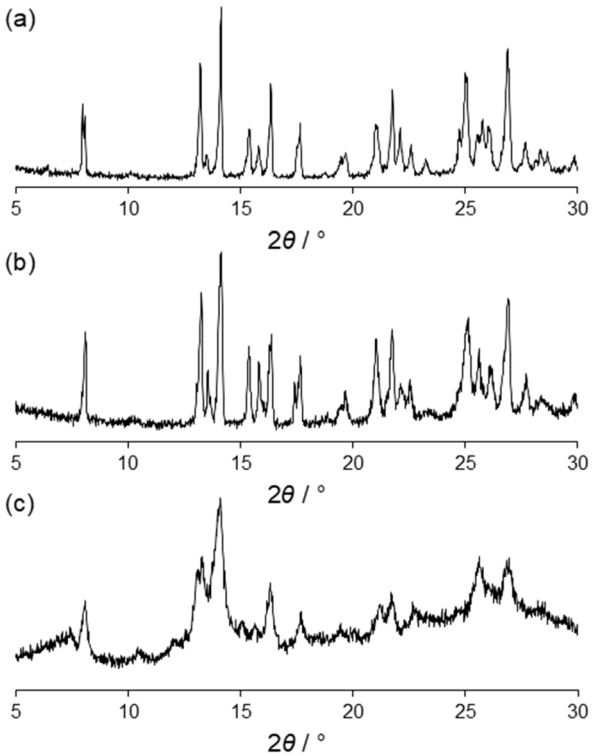

Fig. 5 Powder XRD patterns corresponding to the microcrystalline powders of **1** after filtering (a) and after heating to 300 °C for 1 h (b) and the product obtained from NG and annealing (c).

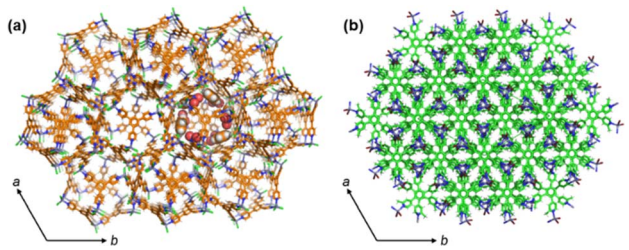

Fig. 6 Crystal structure of a poly-[*n*]-catenane self-assembled of interlocked $M_{12}L_8$ nanocages (a) and the structure of **1** (b). Both structures are viewed along the stacking direction (*c*-axis). Solvent molecules included in one $M_{12}L_8$ cage are shown in the PC-MOCs and have been omitted for clarity in **1**.

reactivity is significant as it shows that the templating effect in the self-assembling process is not crucial, and the structure is formed regardless of the solvent. This was corroborated by the heating experiments showing the stability of the structure without solvent. Also, the solid-state reactivity allows the synthesis of a 2D MOF in a completely solvent-free process, an important strategy for green chemistry.

Polycatenanes made of MOCs *vs.* 2D MOFs using mTPB and $ZnBr_2$

In coordination-driven self-assembling systems, it is known that "small" changes in one of the building blocks either the organic ligands or the metal ions have a strong influence on the final product.[13–15] We have demonstrated that introducing a methyl group into the 2-position of the 4′-pyridyl rings in the triangular panel-like TPB ligand does not promote the formation of the icosahedral $M_{12}L_8$ nanocages in the solid state.

It is worth noting that the presence of the methyl group does not change the coordination vector direction as the lone pairs of the nitrogen atoms are not altered.[15] Also, the rotation of the interring C–C bonds does not influence the directionality of the N lone pairs. In fact, the Zn–N coordination bonds in **1** are formed with a significant rotation of the methylated pyridine rings to avoid repulsion among the halogen atoms and the methyl groups. We note that similar values in the pyridine's rotation θ angles ($\theta = 36°$) have been observed in $M_{12}L_8$ mechanically interlocked nanocages, which are also fundamental to allow guest exchange mechanisms *via* single-crystal-to-single-crystal reactions.[33] Thus, the presence of the methyl group, in our opinion, should not impede the formation of non-interlocked $M_{12}L_8$ nanocages. Moreover, the benzene–benzene aromatic interactions, which play an important role in the mechanical bonds and the formation of the interlocked $M_{12}L_8$ nanocages,[8,13,16] can be also formed in **1**, as seen in Fig. 4.

While the interlocking of $M_{12}L_8$ nanocages might be feasible due to the large openings of the nanocages (window dimensions 13 Å × 22 Å)[8] (Fig. 1a); the constrained environment due to the methyl groups within the mechanical bonds most likely destabilizes a potential structure formed of interlocked $M_{12}L_8$ nanocages. Thus, the presence of methyl groups switches the formation to other structures such as 2D MOFs **1** instead of PC-MOCs, which could be seen as a steric effect, as reported in other coordination-driven self-assembling systems.[34] **mTPB** and **TPB** ligands are both symmetric but introducing the methyl groups induced a change in the potential energy surface (PES) landscape of the ligand. This ligand modification might also influence the electrostatic interactions among the solvent molecules (*i.e.*, the templating effect). This aspect might also have an influence on the crystal packing, forming the 2D MOF instead of the interlocked structure.

However, it is important to note that due to the structural aspects described above, the lattice packing of **1** and the catenane show many similarities. Fig. 6 depicts the structure of PC-MOCs and the 2D MOF **1** viewed along the *c*-axis. The same trigonal symmetry is observed in both structures, which reflects the C_3 high symmetry of both **TPB** and **mTPB** triangular panel-like ligands.

Conclusions

We synthesized a new high symmetry C_3 rigid panel-like triangular ligand (*i.e.*, **mTPB**) and studied its self-assembly with $ZnBr_2$ in the formation of poly-[*n*]-catenanes formed of interlocked $M_{12}L_8$ MOCs. The self-assembly of **mTPB** and $ZnBr_2$ forms a new 2D MOF with porous layers but does not form mechanically interlocked $M_{12}L_8$ under the same crystallization conditions. The solid-state reactivity of **mTPB** and $ZnBr_2$ was explored by grinding and annealing, showing that the 2D MOFs are formed in the absence of a solvent. Structural analysis (SC-

XRD data) reveals that while Zn–N coordination bonds, aromatic–aromatic interactions and symmetry preservation are observed in both 2D MOFs and in PCs-MOCs, and the presence of methyl groups in **mTPB** might be one of the reasons switching the self-assembling components to form the 2D MOF instead of the interlocking of $M_{12}L_8$ nanocages. Further work is aimed at the synthesis of new high-symmetry triangular ligands for the synthesis of interlocked $M_{12}L_8$ including MOCs and polymeric MOFs with different ligands in the solid state.

Data availability

Crystallographic data for the ligand **mTPB** and **1** have been deposited at the CCDC database under accession numbers 2388980 and 2389166, respectively, and can be obtained from **https://www.ccdc.cam.ac.uk/structures/**.

Conflicts of interest

There are no conflicts to declare.

Notes and references

1 T. Friščić, A. V. Trask, W. Jones and W. D. S. Motherwell, *Angew. Chem., Int. Ed.*, 2006, **45**, 7546.
2 G. A. Bowmaker, *Chem. Commun.*, 2013, **49**, 334.
3 S. L. James, C. J. Adams, C. Bolm, D. Braga, P. Collier, T. Friščić, F. Grepioni, K. D. M. Harris, G. Hyett, W. Jones, A. Krebs, J. Mack, L. Maini, A. G. Orpen, I. P. Parkin, W. C. Shearouse, J. W. Steed and D. C. Waddell, *Chem. Soc. Rev.*, 2012, **41**, 413.
4 A. D. Katsenis, A. Puskaric, V. Strukil, C. Mottillo, P. A. Julien, K. Užarević, M.-H. Pham, T.-O. Do, S. A. J. Kimber, P. Lazic, O. Magdysyuk, R. E. Dinnebier, I. Halasz and T. Friščić, *Nat. Commun.*, 2015, **6**, 6662.
5 L. Catalano, L. S. Germann, P. A. Julien, M. Arhangelskis, I. Halasz, K. Uzarevic, M. Etter, R. E. Dinnebier, M. Ursini, M. Cametti, J. Martí-Rujas, T. Friscic, P. Metrangolo, G. Resnati and G. Terraneo, *Chem*, 2021, **7**, 146–154.
6 D. Feng, X. Hao, Z. Fei, P. Huang and F. Guo, *Organometallics*, 2024, **43**, 1640–1646.
7 J. Martí-Rujas and F. Guo, *Dalton Trans.*, 2021, **50**, 11665–11680.
8 S. Torresi, A. Famulari and J. Martí-Rujas, *J. Am. Chem. Soc.*, 2020, **142**, 9537–9543.
9 J. Martí-Rujas, S. Elli and A. Famulari, *Sci. Rep.*, 2023, **13**, 5605.
10 J. Martí-Rujas, S. Elli, A. Sacchetti and F. Castiglione, *Dalton Trans.*, 2021, **51**, 53–58.
11 S. Elli, A. Famulari and J. Marti-Rujas, *ChemPlusChem*, 2024, **89**, e202400332.
12 J. Martí-Rujas, S. Ma and A. Famulari, *Inorg. Chem.*, 2022, **61**, 10863–10871.
13 J. Heine, J. Schmedt auf der Gunne and S. Dehnen, *J. Am. Chem. Soc.*, 2011, **133**, 10018.
14 E. C. Constable, G. Zhang, C. E. Housecroft and J. Zampese, *CrystEngComm*, 2011, **13**, 6864.
15 C. Housecroft and E. C. Constable, *Helv. Chim. Acta*, 2024, **107**, e202400023.
16 J. Martí-Rujas and A. Famulari, *Angew. Chem., Int. Ed*, 2024, **63**, e202407626.
17 S. R. Batten, B. F. Hoskins and R. Robson, *J. Am. Chem. Soc.*, 1995, **117**, 5385.
18 K. Biradha and M. Fujita, *Angew. Chem., Int. Ed.*, 2002, **42**, 3392–3395.
19 Y. Inokuma, T. Arai and M. Fujita, *Nat. Chem.*, 2010, **2**, 780–783.
20 F. Shao, J. Li, J. P. Tong, J. Zhang, M. G. Chen, Z. Zheng, R. B. Huang, L. S. Zheng and J. Tao, *Chem. Commun.*, 2013, **49**, 10730.
21 Q. Jiang, H. Suzuki, Y. Wada, X. Wang, Y. Murakami, T. Matsumoto, P. M. Usov and M. Kawano, *Chem. Commun.*, 2024, **60**, 8236–8239.
22 T. Abe, K. Takeuchi and S. Hiraoka, *Nat. Commun.*, 2024, **15**, 7630–7645.
23 K. Ohara, J. Martí-Rujas, F. Izumi, D. Hashizume, M. Kawano and M. Fujita, *J. Am. Chem. Soc.*, 2009, **131**, 3860–3861.
24 J. Martí-Rujas, N. Islam, D. Hashizume, F. Izumi, M. Fujita and M. Kawano, *J. Am. Chem. Soc.*, 2011, **133**, 5853–5860.
25 T. M. Benneth and A. Cheetham, *Acc. Chem. Res.*, 2014, **47**, 1555–1562.
26 J. Martí-Rujas, *Materials*, 2019, **12**, 4088.
27 G. K. Kole and J. J. Vitta, *Chem. Soc. Rev.*, 2013, **42**, 1755–1775.
28 K. D. M. Harris, M. Tremayne and B. M. Kariuki, *Angew. Chem., Int. Ed.*, 2001, **40**, 1626–1651.
29 J. Martí-Rujas, *Dalton Trans.*, 2020, **49**, 13897–13916.
30 L. Cheng, C. Liang, W. Liu, Y. Wang, B. Chen, H. Zhang, Y. Wang, Z. Chai and S. Wang, *J. Am. Chem. Soc.*, 2020, **142**, 16218–16222.
31 L. J. Barbour, *Chem. Commun.*, 2006, 1163.
32 Q. Liu, X. Li, Y. Wen, Q. Xu, X.-T. Wu and Q.-L. Zhu, *Adv. Mater. Interfaces*, 2020, **7**, 2000813.
33 J. Martí-Rujas, S. Elli, A. Zanotti, A. Famulari and F. Castiglione, *Chem.–Eur. J.*, 2023, **29**, e202302025.
34 S. Watanabe, M. Yamashina, E. Tsurumaki and S. Toyota, *ChemistryEurope*, 2023, **1**, e202300047.